Radboud Repository

Radboud University Nijmegen

PDF hosted at the Radboud Repository of the Radboud University Nijmegen

The following full text is a preprint version which may differ from the publisher's version.

For additional information about this publication click this link.
http://hdl.handle.net/2066/124924

Please be advised that this information was generated on 2019-04-20 and may be subject to change.

EUROPEAN ORGANISATION FOR NUCLEAR RESEARCH

CERN-PPE/96-161
November 18, 1996

Search for the Standard Model Higgs Boson in e^+e^- Collisions at $\sqrt{s} = 161$ GeV

The OPAL Collaboration

Abstract

This letter describes a search for the Standard Model Higgs boson using data from e^+e^- collisions collected at a centre-of-mass energy of 161 GeV by the OPAL detector at LEP. The data correspond to an integrated luminosity of 10.0 pb^{-1}. The search is sensitive to the main final states from the process where the Higgs boson is produced in association with a fermion anti-fermion pair, namely four jets, two jets with missing energy, and two jets produced together with a pair of electrons, muons or tau leptons. Two candidate events are observed, in agreement with Standard Model background expectations. In combination with previous OPAL searches at centre-of-mass energies close to the Z^0 resonance, we derive a lower limit of 65.0 GeV for the mass of the Standard Model Higgs boson, at the 95% confidence level.

To be submitted to Physics Letters B

The OPAL Collaboration

K. Ackerstaff[8], G. Alexander[23], J. Allison[16], N. Altekamp[5], K. Ametewee[25], K.J. Anderson[9], S. Anderson[12], S. Arcelli[2], S. Asai[24], D. Axen[29], G. Azuelos[18,a], A.H. Ball[17], E. Barberio[8], R.J. Barlow[16], R. Bartoldus[3], J.R. Batley[5], J. Bechtluft[14], C. Beeston[16], T. Behnke[8], A.N. Bell[1], K.W. Bell[20], G. Bella[23], S. Bentvelsen[8], P. Berlich[10], S. Bethke[14], O. Biebel[14], A. Biguzzi[2], V. Blobel[27], I.J. Bloodworth[1], J.E. Bloomer[1], M. Bobinski[10], P. Bock[11], H.M. Bosch[11], M. Boutemeur[34], B.T. Bouwens[12], S. Braibant[12], R.M. Brown[20], H.J. Burckhart[8], C. Burgard[8], R. Bürgin[10], P. Capiluppi[2], R.K. Carnegie[6], A.A. Carter[13], J.R. Carter[5], C.Y. Chang[17], D.G. Charlton[1,b], D. Chrisman[4], P.E.L. Clarke[15], I. Cohen[23], J.E. Conboy[15], O.C. Cooke[16], M. Cuffiani[2], S. Dado[22], C. Dallapiccola[17], G.M. Dallavalle[2], S. De Jong[12], L.A. del Pozo[8], K. Desch[3], M.S. Dixit[7], E. do Couto e Silva[12], M. Doucet[18], E. Duchovni[26], G. Duckeck[34], I.P. Duerdoth[16], J.E.G. Edwards[16], P.G. Estabrooks[6], H.G. Evans[9], M. Evans[13], F. Fabbri[2], P. Fath[11], F. Fiedler[27], M. Fierro[2], H.M. Fischer[3], R. Folman[26], D.G. Fong[17], M. Foucher[17], A. Fürtjes[8], P. Gagnon[7], J.W. Gary[4], J. Gascon[18], S.M. Gascon-Shotkin[17], N.I. Geddes[20], C. Geich-Gimbel[3], T. Geralis[20], G. Giacomelli[2], P. Giacomelli[4], R. Giacomelli[2], V. Gibson[5], W.R. Gibson[13], D.M. Gingrich[30,a], D. Glenzinski[9], J. Goldberg[22], M.J. Goodrick[5], W. Gorn[4], C. Grandi[2], E. Gross[26], J. Grunhaus[23] M. Gruwé[8], C. Hajdu[32], G.G. Hanson[12], M. Hansroul[8], M. Hapke[13], C.K. Hargrove[7], P.A. Hart[9], C. Hartmann[3], M. Hauschild[8], C.M. Hawkes[5], R. Hawkings[8], R.J. Hemingway[6], M. Herndon[17], G. Herten[10], R.D. Heuer[8], M.D. Hildreth[8], J.C. Hill[5], S.J. Hillier[1], T. Hilse[10], P.R. Hobson[25], R.J. Homer[1], A.K. Honma[28,a], D. Horváth[32,c], R. Howard[29], R.E. Hughes-Jones[16], D.E. Hutchcroft[5], P. Igo-Kemenes[11], D.C. Imrie[25], M.R. Ingram[16], K. Ishii[24], A. Jawahery[17], P.W. Jeffreys[20], H. Jeremie[18], M. Jimack[1], A. Joly[18], C.R. Jones[5], G. Jones[16], M. Jones[6], R.W.L. Jones[8], U. Jost[11], P. Jovanovic[1], T.R. Junk[8], D. Karlen[6], K. Kawagoe[24], T. Kawamoto[24], R.K. Keeler[28], R.G. Kellogg[17], B.W. Kennedy[20], B.J. King[8], J. Kirk[29], S. Kluth[8], T. Kobayashi[24], M. Kobel[10], D.S. Koetke[6], T.P. Kokott[3], M. Kolrep[10], S. Komamiya[24], T. Kress[11], P. Krieger[6], J. von Krogh[11], P. Kyberd[13], G.D. Lafferty[16], R. Lahmann[17], W.P. Lai[19], D. Lanske[14], J. Lauber[15], S.R. Lautenschlager[31], J.G. Layter[4], D. Lazic[22], A.M. Lee[31], E. Lefebvre[18], D. Lellouch[26], J. Letts[2], L. Levinson[26], C. Lewis[15], S.L. Lloyd[13], F.K. Loebinger[16], G.D. Long[17], M.J. Losty[7], J. Ludwig[10], M. Mannelli[8], S. Marcellini[2], C. Markus[3], A.J. Martin[13], J.P. Martin[18], G. Martinez[17], T. Mashimo[24], W. Matthews[25], P. Mättig[3], W.J. McDonald[30], J. McKenna[29], E.A. Mckigney[15], T.J. McMahon[1], A.I. McNab[13], R.A. McPherson[8], F. Meijers[8], S. Menke[3], F.S. Merritt[9], H. Mes[7], J. Meyer[27], A. Michelini[2], G. Mikenberg[26], D.J. Miller[15], R. Mir[26], W. Mohr[10], A. Montanari[2], T. Mori[24], M. Morii[24], U. Müller[3], K. Nagai[26], I. Nakamura[24], H.A. Neal[8], B. Nellen[3], B. Nijjhar[16], R. Nisius[8], S.W. O'Neale[1], F.G. Oakham[7], F. Odorici[2], H.O. Ogren[12], N.J. Oldershaw[16], T. Omori[24], M.J. Oreglia[9], S. Orito[24], J. Pálinkás[33,d], G. Pásztor[32], J.R. Pater[16], G.N. Patrick[20], J. Patt[10], M.J. Pearce[1], S. Petzold[27], P. Pfeifenschneider[14], J.E. Pilcher[9], J. Pinfold[30], D.E. Plane[8], P. Poffenberger[28], B. Poli[2], A. Posthaus[3], H. Przysiezniak[30], D.L. Rees[1], D. Rigby[1], S. Robertson[28], S.A. Robins[13], N. Rodning[30], J.M. Roney[28], A. Rooke[15], E. Ros[8], A.M. Rossi[2], M. Rosvick[28], P. Routenburg[30], Y. Rozen[22], K. Runge[10], O. Runolfsson[8], U. Ruppel[14], D.R. Rust[12], R. Rylko[25], K. Sachs[10], E.K.G. Sarkisyan[23], M. Sasaki[24], C. Sbarra[2], A.D. Schaile[34], O. Schaile[34], F. Scharf[3],

P. Scharff-Hansen[8], P. Schenk[27], B. Schmitt[8], S. Schmitt[11], M. Schröder[8], H.C. Schultz-Coulon[10], M. Schulz[8], M. Schumacher[3], P. Schütz[3], W.G. Scott[20], T.G. Shears[16], B.C. Shen[4], C.H. Shepherd-Themistocleous[8], P. Sherwood[15], G.P. Siroli[2], A. Sittler[27], A. Skillman[15], A. Skuja[17], A.M. Smith[8], T.J. Smith[28], G.A. Snow[17], R. Sobie[28], S. Söldner-Rembold[10], R.W. Springer[30], M. Sproston[20], A. Stahl[3], M. Steiert[11], K. Stephens[16], J. Steuerer[27], B. Stockhausen[3], D. Strom[19], F. Strumia[8], P. Szymanski[20], R. Tafirout[18], S.D. Talbot[1], S. Tanaka[24], P. Taras[18], S. Tarem[22], M. Thiergen[10], M.A. Thomson[8], E. von Törne[3], S. Towers[6], I. Trigger[18], T. Tsukamoto[24], E. Tsur[23], A.S. Turcot[9], M.F. Turner-Watson[8], P. Utzat[11], R. Van Kooten[12], M. Verzocchi[10], P. Vikas[18], M. Vincter[28], E.H. Vokurka[16], F. Wäckerle[10], A. Wagner[27], C.P. Ward[5], D.R. Ward[5], J.J. Ward[15], P.M. Watkins[1], A.T. Watson[1], N.K. Watson[7], P.S. Wells[8], N. Wermes[3], J.S. White[28], B. Wilkens[10], G.W. Wilson[27], J.A. Wilson[1], G. Wolf[26], S. Wotton[5], T..R. Wyatt[16], S. Yamashita[24], G. Yekutieli[26], V. Zacek[18]

[1]School of Physics and Space Research, University of Birmingham, Birmingham B15 2TT, UK
[2]Dipartimento di Fisica dell' Università di Bologna and INFN, I-40126 Bologna, Italy
[3]Physikalisches Institut, Universität Bonn, D-53115 Bonn, Germany
[4]Department of Physics, University of California, Riverside CA 92521, USA
[5]Cavendish Laboratory, Cambridge CB3 0HE, UK
[6] Ottawa-Carleton Institute for Physics, Department of Physics, Carleton University, Ottawa, Ontario K1S 5B6, Canada
[7]Centre for Research in Particle Physics, Carleton University, Ottawa, Ontario K1S 5B6, Canada
[8]CERN, European Organisation for Particle Physics, CH-1211 Geneva 23, Switzerland
[9]Enrico Fermi Institute and Department of Physics, University of Chicago, Chicago IL 60637, USA
[10]Fakultät für Physik, Albert Ludwigs Universität, D-79104 Freiburg, Germany
[11]Physikalisches Institut, Universität Heidelberg, D-69120 Heidelberg, Germany
[12]Indiana University, Department of Physics, Swain Hall West 117, Bloomington IN 47405, USA
[13]Queen Mary and Westfield College, University of London, London E1 4NS, UK
[14]Technische Hochschule Aachen, III Physikalisches Institut, Sommerfeldstrasse 26-28, D-52056 Aachen, Germany
[15]University College London, London WC1E 6BT, UK
[16]Department of Physics, Schuster Laboratory, The University, Manchester M13 9PL, UK
[17]Department of Physics, University of Maryland, College Park, MD 20742, USA
[18]Laboratoire de Physique Nucléaire, Université de Montréal, Montréal, Quebec H3C 3J7, Canada
[19]University of Oregon, Department of Physics, Eugene OR 97403, USA
[20]Rutherford Appleton Laboratory, Chilton, Didcot, Oxfordshire OX11 0QX, UK
[22]Department of Physics, Technion-Israel Institute of Technology, Haifa 32000, Israel
[23]Department of Physics and Astronomy, Tel Aviv University, Tel Aviv 69978, Israel
[24]International Centre for Elementary Particle Physics and Department of Physics, University

of Tokyo, Tokyo 113, and Kobe University, Kobe 657, Japan
[25]Brunel University, Uxbridge, Middlesex UB8 3PH, UK
[26]Particle Physics Department, Weizmann Institute of Science, Rehovot 76100, Israel
[27]Universität Hamburg/DESY, II Institut für Experimental Physik, Notkestrasse 85, D-22607 Hamburg, Germany
[28]University of Victoria, Department of Physics, P O Box 3055, Victoria BC V8W 3P6, Canada
[29]University of British Columbia, Department of Physics, Vancouver BC V6T 1Z1, Canada
[30]University of Alberta, Department of Physics, Edmonton AB T6G 2J1, Canada
[31]Duke University, Dept of Physics, Durham, NC 27708-0305, USA
[32]Research Institute for Particle and Nuclear Physics, H-1525 Budapest, P O Box 49, Hungary
[33]Institute of Nuclear Research, H-4001 Debrecen, P O Box 51, Hungary
[34]Ludwigs-Maximilians-Universität München, Sektion Physik, Am Coulombwall 1, D-85748 Garching, Germany

[a] and at TRIUMF, Vancouver, Canada V6T 2A3
[b] and Royal Society University Research Fellow
[c] and Institute of Nuclear Research, Debrecen, Hungary
[d] and Department of Experimental Physics, Lajos Kossuth University, Debrecen, Hungary

1 Introduction

Locally gauge-invariant theories of the electroweak interaction introduce spontaneous symmetry breaking to allow some of the gauge bosons to acquire mass while keeping the theory renormalizable. The Standard Model (SM) [1] is the simplest such theory and uses the self-interaction of a single doublet of complex scalar fields [2] to effect spontaneous symmetry breaking. This model predicts the existence of one physical scalar particle, the Higgs boson, H^0, whose couplings are fixed but whose mass is not predicted. Despite a wide experimental effort, the Higgs boson has not yet been discovered. The current experimental lower limits for its mass, m_{H^0}, obtained from large samples of Z^0 boson decays, are in the vicinity of 60 GeV [3] [4].

During the summer of 1996 the centre-of-mass energy of the LEP e^+e^- collider was upgraded to 161 GeV. The higher energy increases the sensitivity of the searches for the SM Higgs boson with mass in the region of the current limits. At this centre-of-mass energy, the main production process for the SM Higgs boson is $e^+e^- \to Z^0H^0$. The dominant decay is $H^0 \to b\bar{b}$, with a branching ratio of approximately 86%. Other relevant decay modes are: $H^0 \to \tau^+\tau^-$ (8%), $H^0 \to c\bar{c}$ (4%), and $H^0 \to$gluons (2%) [5]. In the mass range of interest, these branching ratios exhibit only a mild dependence on the Higgs boson mass.

The searches described address the principal final state topologies, namely: (i) the four-jet channel, $e^+e^- \to Z^0H^0 \to q\bar{q}b\bar{b}$; (ii) the missing energy channel, mainly from $e^+e^- \to Z^0H^0 \to \nu\bar{\nu}q\bar{q}$, but including a small contribution from the W^+W^- fusion process $e^+e^- \to \nu\bar{\nu}H^0$; (iii) the tau

channels, $e^+e^- \to Z^0H^0 \to \tau^+\tau^- q\bar{q}$ and $q\bar{q}\tau^+\tau^-$; (iv) the electron and muon channels, predominantly from $e^+e^- \to Z^0H^0 \to e^+e^- q\bar{q}$ and $\mu^+\mu^- q\bar{q}$, but including a small contribution from the Z^0Z^0 fusion process $e^+e^- \to e^+e^- H^0$. These topologies account for about 95% of all Higgs boson final states.

2 Detector, Data, and Simulations

This analysis uses 10.0 pb^{-1} of data recorded with the OPAL detector [6], at an e^+e^- centre-of-mass energy, $\sqrt{s}$, of 161.3 ± 0.2 GeV. OPAL is a multipurpose apparatus with nearly complete solid angle coverage and excellent hermeticity. The central tracking detector consists of two layers of silicon microstrip detectors [7] with polar angle[1] coverage $|\cos\theta| < 0.9$, which immediately surround the beam-pipe, followed by a high-precision vertex drift chamber, a large-volume jet chamber, and z-chambers, all in a uniform 0.435 T axial magnetic field. A lead-glass electromagnetic calorimeter is located outside the magnet coil, which, in combination with the forward calorimeter, gamma catcher, and silicon-tungsten luminometer [8], complete the geometrical acceptance down to 24 mrad from the beam direction. The silicon-tungsten luminometer serves to measure the integrated luminosity using small-angle Bhabha scattering events [9]. The magnet return yoke is instrumented with streamer tubes for hadron calorimetry and is surrounded by several layers of muon chambers. Events are reconstructed from charged-particle tracks and energy deposits ("clusters") in the electromagnetic and hadronic calorimeters. The tracks and clusters have to pass a set of quality requirements similar to those used in previous Higgs boson searches [10]. In calculating the total visible energies and momenta, $E_{\rm vis}$ and $\vec{P}_{\rm vis}$, of events and of individual jets, corrections are applied which reduce the effect of double-counting of energy in the case of tracks and associated clusters.

The signal detection efficiencies and accepted background cross-sections are estimated using a variety of Monte Carlo samples all processed through a full simulation [11] of the OPAL detector. The HZHA generator [12], including initial-state radiation effects, is used to simulate Higgs boson production processes. The generated partons are hadronized using JETSET [13]. Signal samples are produced for fixed values of $m_{\rm H^0}$ between 35 GeV and 70 GeV. The estimates of the different background processes are based primarily on the following event generators: PYTHIA [13] ($Z^0/\gamma^* \to q\bar{q}(\gamma)$), EXCALIBUR [14] (four-fermion processes), BHWIDE [15] ($e^+e^-(\gamma)$), KORALZ [16] ($\mu^+\mu^-(\gamma)$ and $\tau^+\tau^-(\gamma)$), PHOJET [17] and Vermaseren [18] (hadronic and leptonic two-photon processes).

[1] OPAL uses a right-handed coordinate system where the $+z$ direction is along the electron beam and where $+x$ points to the centre of the LEP ring. The polar angle, θ, is defined with respect to the $+z$ direction and the azimuthal angle, ϕ, with respect to the horizontal, $+x$ direction.

3 The Four-Jet Channel

The process $e^+e^- \to Z^0H^0 \to q\bar{q}b\bar{b}$ gives rise to approximately 60% of the Higgs boson signal topologies. It is characterized by four energetic hadronic jets, large visible energy, and the presence of displaced secondary vertices signalling b-hadron decays. The backgrounds are $Z^0/\gamma^* \to q\bar{q}$ with or without initial state radiation and accompanied by hard gluon emission, four-fermion processes, in particular $e^+e^- \to W^+W^-$, and two-photon processes. The suppression of these backgrounds relies on kinematic reconstruction of the Z^0 boson in the hadronic $q\bar{q}$ system, and on the identification of b-quarks from the Higgs boson decay. The tagging of particles containing b-quarks proceeds by detecting displaced secondary vertices in three dimensions using the high-resolution silicon microvertex detector.

(1) The events must qualify as hadronic final states as described in Ref. [19].

(2) The radiative process $e^+e^- \to Z^0\gamma \to q\bar{q}\gamma$ is largely eliminated by requiring that the effective centre-of-mass energy, $\sqrt{s'}$, obtained by discarding from the event the radiative photon following Ref. [20], be at least 140 GeV. Also, the visible mass, $M_{\rm vis}$, calculated using the total visible energy and momentum of the event, is required to lie between 120 GeV and 200 GeV.

(3) The events are reconstructed into four jets using the Durham algorithm [21]. The jet resolution parameter, y_{34}, at which the number of jets changes from 3 to 4, is required to be larger than 0.005. All four jets are required to contain at least two tracks and two electromagnetic calorimeter clusters. To discriminate against poorly reconstructed events, a kinematic fit, using energy and momentum conservation constraints, is required to yield a χ^2 probability larger than 0.01. The jet energies and directions resulting from this fit are used in cuts (4) and (5) below.

(4) The $Z^0/\gamma^* \to q\bar{q}$ background is further suppressed by requiring that the C parameter [22] be larger than 0.45, and that all jet-jet pairs have an opening angle of at least 40° and an invariant mass larger than 25 GeV.

(5) Events are rejected if they are compatible with the process $e^+e^- \to W^+W^-$. The two jets having the largest opening angle are assigned to one of the $W^\pm$ bosons and the two remaining jets to the other. An event is rejected if both jet pairs have an invariant mass between 70 GeV and 90 GeV.

(6) The $e^+e^- \to H^0Z^0$ hypothesis is tested by a kinematic fit which, in addition to the energy and momentum conservation constraints, also requires that two of the four jets have an invariant mass equal to the Z^0 boson mass, m_{Z^0}. This fit is applied in turn to all six possible associations of the four jets to the Z^0 and H^0 bosons. The combination yielding the highest χ^2 probability is selected, and this probability is required to be larger than 0.01.

(7) To suppress the remaining background, at least one of the two jets associated with the Higgs boson decay is required to show evidence for b-quark flavour. Secondary decay

vertices are identified in each jet separately, using two complementary methods described in [23] and [24], and their decay length significances, S, are calculated. The decay length significance is defined as $S = \ell/\sigma_\ell$ where ℓ is the distance, in three dimensions, between the primary and the secondary vertex, and σ_ℓ the error assigned to ℓ. The jets assigned to the Higgs boson decay must satisfy at least one of the following conditions: (i) the sum of the two decay length significances for each of the two jets according to [23] is larger than 5; (ii) at least one of the two jets has a secondary vertex, identified according to [24], with more than three tracks and having S larger than 10.

Distributions of $\sqrt{s'}$, y_{34}, and S are shown in Figures 1(a), (b), and (c) for data and Monte Carlo. In the case of Figure 1(c), calibration data collected in 1996 at $\sqrt{s}$ =m_{Z^0}, and a corresponding Monte Carlo sample, are shown. The agreement in their distributions demonstrates the adequate modelling of secondary vertices. The numbers of expected events, estimated from Monte Carlo at each stage of the selection, are compared with the data in Table 1. As an example, the detection efficiencies for a 65 GeV Higgs boson are also listed; the efficiencies for other values of m_{H^0} can be found in Table 5. The background predictions are cross-checked using the HERWIG [25], ARIADNE [26] and grc4f [27] generators, which yield statistically consistent results.

The selection retains one data event, which is consistent with the predicted background of 0.8 ± 0.1 events. The candidate event has $y_{34} = 0.0054$ and $C = 0.48$. The invariant mass of the two jets associated with the Higgs boson decay (see Figure 1(d)) is 46.6 ± 3.1 GeV, and one of these jets has a secondary vertex with $S = 13.7$.

Cut	Data	Total bkg.	$\mathrm{q\bar{q}}(\gamma)$	4-ferm.	$\gamma\gamma$	Efficiency (%) $m_{\mathrm{H}^0} = 65$ GeV
(1)	1500	1443.9	1345.9	52.5	45.5	99.9
(2)	373	362.2	336.9	24.9	0.4	91.3
(3)	45	39.8	27.8	12.1	0	77.2
(4)	25	21.3	12.0	9.3	0	62.2
(5)	16	16.1	11.3	4.9	0	49.7
(6)	11	12.0	7.7	4.3	0	45.3
(7)	1	0.8 ± 0.1	0.6	0.2	0	22.8

Table 1: *The numbers of events after each cut for the data and the expected background in the four-jet channel. The background estimates are normalised to 10.0* pb^{-1}. *The quoted error is statistical. The last column shows the selection efficiencies for the* $\mathrm{Z}^0\mathrm{H}^0 \to \mathrm{q\bar{q}b\bar{b}}$ *final state, for a 65 GeV Higgs boson. The small discrepancy between the data and the total backgrounds in the first line is due to an incomplete modelling of two-photon processes.*

The signal detection efficiencies quoted for this channel in Table 5 are affected by the following uncertainties: Monte Carlo statistics, 3%; simulation of the Higgs boson decay with regards to fragmentation and hadronization, 0.3%; modelling of the cut variables other than

those used for b-tagging, 3.7%; b-tagging (uncertainties from modelling the beam spot and track parameter resolutions, b-hadron fragmentation and lifetimes), 4.8%; uncertainty from the centre-of-mass energy, 0.2%. Taking these uncertainties as independent and adding them in quadrature results in a total systematic uncertainty of 6.7% (relative error).

4 The Missing Energy Channel

The $\nu\bar{\nu}q\bar{q}$ final-state topology arises mainly from the process $e^+e^-\to Z^0H^0\to\nu\bar{\nu}q\bar{q}$, with a branching ratio of approximately 18%, but includes a small contribution from the W^+W^- fusion process $e^+e^-\to\nu\bar{\nu}H^0\to\nu\bar{\nu}q\bar{q}$ (4.3% relative contribution, for m_{H^0}=65 GeV). These events are characterized by large missing momentum and two energetic, acoplanar, hadronic jets. The dominant backgrounds are mismeasured $Z^0/\gamma^*\to q\bar{q}$ events, four-fermion processes with a neutrino in the final state, such as $W^+W^-\to\ell^\pm\nu q\bar{q}$ and $W^\pm e^\mp\nu\to q\bar{q}\ e^\mp\nu$, and events in which particles go undetected down the beam pipe such as $e^+e^-\to Z^0\gamma$ and two-photon events. For most of these backgrounds, the missing momentum vector points close to the beam direction, while the signal events tend to have missing momentum in the transverse plane. The event selection exploits this difference.

(1) To reduce two-photon and beam-wall interactions, a preselection is applied. There must be more than six tracks which pass the quality cuts, and the number of such tracks must exceed 20% of the total number of tracks in the event. The energy deposited in the forward detector, gamma catcher and silicon-tungsten luminometer must be less than 2 GeV, 5 GeV, and 5 GeV, respectively. The fraction of energy deposited in the region $|\cos\theta| > 0.9$ must not exceed 30% of the total visible energy in the event. The total transverse momentum of the event, $P^T_{\rm vis}$, must be greater than 1 GeV and the visible mass must satisfy $M_{\rm vis} > 4$ GeV.

(2) To remove backgrounds in which particles go undetected down the beam pipe, the polar angle, $\theta_{\rm miss}$, of the missing momentum ($\vec{P}_{\rm miss} = -\vec{P}_{\rm vis}$) must satisfy $|\cos\theta_{\rm miss}| < 0.9$. The z component of the visible momentum, $P^z_{\rm vis}$, is required to be less than 30 GeV.

(3) Many of the $e^+e^-\to Z^0\gamma$ events in which the photon is within the detector acceptance will survive the previous cut. Vetoing events in which an isolated photon[2] with energy greater than 30 GeV has been identified efficiently removes this background.

(4) The remaining two-photon background is eliminated by requiring $P^T_{\rm vis} > 8$ GeV. As a precaution against large fluctuations in the measured hadronic energy, $P^T_{\rm vis}$ is recalculated excluding hadronic calorimeter clusters and is also required to be larger than 5 GeV.

(5) The remaining events are reconstructed as two-jet events using the Durham algorithm. The jet resolution parameter, y_{23}, at which the event changes from the two-jet to the three-

[2]An isolated photon is defined here either as an electromagnetic cluster with no track within a cone of 20° half-angle around it, or as an identified photon conversion [28] satisfying the same isolation criterion.

jet topology is required to be less than 0.05; this reduces the $Z^0/\gamma^* \to q\bar{q}$ background. Both jets are required to have a polar angle satisfying $|\cos\theta| < 0.9$, to ensure good containment.

(6) The dominant remaining background is from $Z^0/\gamma^* \to q\bar{q}$ events in which the two jets tend to be back-to-back, in contrast to signal events in which the jets are expected to be acoplanar. This background is suppressed by requiring that the jet-jet acoplanarity angle be larger than 8°. The acoplanarity angle is defined as $180° - \phi_{jj}$ where ϕ_{jj} is the angle between the two jets in the plane transverse to the beam direction.

(7) To reduce four-fermion backgrounds which include an intermediate, on-shell, vector boson, the selected events are required to satisfy $M_{\rm vis} < 75$ GeV.

Distributions of $M_{\rm vis}$, $P^T_{\rm vis}$ and of the acoplanarity angle are shown in Figures 2 (a), (b), and (c). The numbers of observed and expected events after each stage of the selection are given in Table 2, along with the detection efficiency for a 65 GeV Higgs boson. One event survives all cuts, which is consistent with the background expectation of 0.9 ± 0.1 events. The surviving event has $P^T_{\rm vis} = 39.1$ GeV, $E_{\rm vis} = 53.1$ GeV, and $M_{\rm vis} = 37.0$ GeV (see Figure 2(d)). After corrections, the mass of the event is 39.3 ± 4.9 GeV, while the missing mass is 96.1 ± 10.0 GeV. These properties are compatible with those of the process $e^+e^- \to Z^0 + Z^0/\gamma^* \to \nu\bar{\nu}q\bar{q}$.

The detection efficiencies as a function of the Higgs boson mass are listed in Table 5. These include a small correction due to accelerator-related backgrounds in the forward detectors which are not fully simulated. The detection efficiencies are affected by the following uncertainties: Monte Carlo statistics, 2%; uncertainties from fragmentation and hadronization, 1.5%; from modelling the cut variables, 3%. Taking these uncertainties as independent and adding them in quadrature results in a total systematic uncertainty of 4% (relative error).

Cut	Data	Total bkg.	$q\bar{q}(\gamma)$	4-ferm.	$\gamma\gamma$	Efficiency (%) $m_{H^0} = 65$ GeV
(1)	2055	1936.5	778.2	38.0	1120.1	80.5
(2)	1068	1047.7	332.1	28.5	687.0	71.6
(3)	1002	989.6	274.9	27.7	686.9	71.6
(4)	166	146.9	128.7	18.0	0.2	67.1
(5)	134	116.8	109.4	7.2	0.2	56.4
(6)	7	6.6	2.4	4.1	0.1	47.6
(7)	1	0.9±0.1	0.2	0.7	0.1	46.0

Table 2: *The numbers of events after each cut for the data and the expected background for the missing energy channel. The background estimates are normalised to 10.0* $\rm pb^{-1}$*. The quoted error is statistical. The last column shows the selection efficiencies for the* $\nu\bar{\nu}(H^0 \to$ *all) final state, for a 65 GeV Higgs boson. The small discrepancy between the data and the total background in the first line is due to an incomplete modelling of two-photon processes.*

5 The Tau Channels

The $\tau^+\tau^-q\bar{q}$ final state can be produced via the processes $e^+e^-\to Z^0H^0\to\tau^+\tau^-q\bar{q}$ and $q\bar{q}\tau^+\tau^-$, with a total branching ratio of approximately 9%. This analysis is sensitive to both processes, which are characterized by a pair of tau leptons and a pair of energetic hadronic jets. In addition, either the pair of hadronic jets or the pair of tau leptons should have an invariant mass consistent with the Z^0 mass. These characteristics are used to suppress the backgrounds, predominantly from $Z^0/\gamma^*\to q\bar{q}$ and four-fermion processes.

The selection begins with the identification of tau leptons, using any of the three algorithms described below, which address different decay channels of the tau leptons.

(a) An electron, identified by a neural network algorithm [29] and satisfying the fiducial requirement $|\cos\theta| < 0.97$, is classified as a $\tau^\pm\to e^\pm\nu\bar{\nu}$ decay if its momentum is larger than 2 GeV, and if it is isolated. In particular, the number of electromagnetic clusters within a cone of 26° half-angle around the electron track, $N_{\rm em}^{26}$, must be less than six, and the ratio of the electromagnetic energy within an 11° cone to that within a 30° cone, $R_{\rm em}^{11/30}$, must be greater than 0.7. There must be no hadronic calorimeter cluster with energy greater than 0.6 GeV associated with the electron track. Electrons from photon conversions are rejected using a neural network algorithm [28].

(b) A muon, identified using standard selection algorithms [30] and satisfying the fiducial requirement $|\cos\theta| < 0.97$, is classified as a $\tau^\pm\to\mu^\pm\nu\bar{\nu}$ decay if its momentum is larger than 3 GeV, and if it is isolated. In particular, $N_{\rm em}^{26} < 5$, and the ratio of the scalar sum of all track momenta within an 11° cone to that within a 30° cone must be greater than 0.7.

(c) The remaining tau lepton decays are identified as narrow, isolated jets. Jets are reconstructed using a cone algorithm [31] with a half-angle of 23° and with at least 3 GeV of associated energy. Within each resulting jet, a narrow sub-jet of 11° half-angle and having the highest energy is formed in an iterative procedure. The narrow sub-jets are accepted as tau candidates if they satisfy the fiducial requirement $|\cos\theta| < 0.92$, have one or three associated tracks, have an invariant mass less than 3.5 GeV, and are isolated, with $R_{\rm em}^{11/30} > 0.6$.

In the selection that follows, the tau lepton momentum is approximated by the momentum of the visible decay products. When there are two tau lepton candidates with momentum vectors separated by less than 23°, one being identified as a leptonic decay (algorithms (a) or (b)) and one as a narrow jet (algorithm (c)), the candidate identified as a leptonic decay is selected.

(1) To be retained, the events are required to have at least two tau lepton candidates, each with charge of $|q| = 1$.

(2) The total track multiplicity of the event must exceed eight.

(3) Most of the two-photon and $e^+e^-\to Z^0\gamma$ background events are eliminated by requiring that the energy in the forward detector, gamma catcher, and silicon-tungsten luminometer

be less than 4, 10, and 10 GeV, respectively, that $|\cos\theta_{\rm miss}| < 0.97$ and that $P^T_{\rm vis} > 3$ GeV. In addition, the scalar sum of all track and cluster transverse momenta is required to be larger than 40 GeV.

(4) The remaining $Z^0/\gamma^* \to q\bar{q}$ background, with and without radiation, is partially suppressed by requiring that events contain at least four jets, reconstructed using the cone algorithm with a 23° half-angle as in (c) above (single electrons and muons from tau lepton decays are recognized as low-multiplicity "jets"). Events with an energetic isolated photon[3] are removed.

(5) In signal events, the algorithms (a), (b), and (c) identify 2.3 tau candidates on average. Fake candidate pairs are removed by requiring that their sum of charges be zero and that they satisfy a pairwise isolation, $|\cos\alpha_1 \cdot \cos\alpha_2| < 0.8$, where α_i is the angle between the direction of the ith tau candidate and that of the nearest track not associated with it. In those instances where more than one candidate pair passes the selection, the pair with the lowest track multiplicity is chosen and, in case of ambiguity, the one with the lowest value of $|\cos\alpha_1 \cdot \cos\alpha_2|$.

The hadronic part of the event, obtained by excluding the selected tau lepton pair, is then split into two jets using the Durham algorithm. The invariant masses of the tau lepton pair, $m_{\tau\tau}$, and of the hadron jets, $m_{\rm had}$, are calculated using only the tau lepton and jet momentum directions and requiring energy and momentum conservation. At this point the selection separates into two parts, one (A) sensitive to the $Z^0H^0 \to \tau^+\tau^- q\bar{q}$ final state and another (B) sensitive to the $Z^0H^0 \to q\bar{q}\tau^+\tau^-$ final state.

(6) Case A: The selected events must satisfy 75 GeV$< m_{\tau\tau} <$ 105 GeV and $m_{\rm had} >$30 GeV. In addition, $E_{\rm vis}$ is required to be less than 145 GeV, since the neutrinos from the tau lepton decays, originating from the Z^0 boson, give rise to a relatively large missing energy. Finally, cuts are implemented to suppress specific four-fermion backgrounds, from $e^+e^- \to Z^0/\gamma^* + Z^0/\gamma^*$ and $e^+e^- \to Z^0e^+e^-$. If the tau lepton candidates are both classified as $\tau^\pm \to e^\pm\nu\bar{\nu}$ or both as $\tau^\pm \to \mu^\pm\nu\bar{\nu}$, their opening angle is required to be larger than 90° and, in the first case, neither electron is allowed to lie within 36° of the beam axis.

Case B: The selected events must satisfy 75 GeV$< m_{\rm had} <$ 105 GeV and $m_{\tau\tau} >$ 30 GeV. Since in this case the mass cuts are less effective against the background, the requirements on the properties of the tau lepton candidates are tightened. The opening angle of the tau lepton pair must be larger than 110° and, if one of the tau candidates has a track multiplicity exceeding two, the pairwise isolation cut is tightened to $|\cos\alpha_1 \cdot \cos\alpha_2| < 0.55$. Furthermore, to suppress four-fermion backgrounds, pairs with leptons of the same flavour are rejected. Finally, to suppress the process $W^+W^- \to \ell\nu q\bar{q}$, events are rejected if they contain any track or cluster with an energy exceeding 40 GeV.

[3] An energetic isolated photon is defined in this context as an electromagnetic cluster with energy larger than 15 GeV and no track within a cone of 30° half-angle.

Distributions of $|\cos\alpha_1 \cdot \cos\alpha_2|$ and $m_{\tau\tau}$ are shown in Figures 3 (a) and (b) for the data, the backgrounds, and for a 65 GeV Higgs boson signal. The numbers of observed and expected events after each stage of the selection are given in Table 3. The detection efficiency for a 65 GeV Higgs boson is also given. No candidate event is observed while the background is estimated to be 0.16 ± 0.04 events.

The detection efficiencies as a function of the Higgs boson mass are given in Table 5. These include a small correction coming from accelerator-related backgrounds in the forward detectors which are not fully simulated. The detection efficiencies are affected by the following uncertainties: Monte Carlo statistics, 2.8%; uncertainty in the tau lepton identification efficiency, 2%; uncertainties in the modelling of cut variables excluding the tau lepton identification, 6% (case A) and 4% (case B); uncertainties in the modelling of fragmentation and hadronization, 1.2%. Taking these uncertainties as independent and adding them in quadrature results in a total systematic uncertainty of 7% (case A) and 6% (case B) (relative errors).

Cut	Data	Total bkg.	$q\bar{q}(\gamma)$	4-ferm.	$\gamma\gamma$	$\ell^+\ell^-$	ϵ(%), case A 65 GeV	ϵ(%), case B 65 GeV
(1)	858	778.4	95.6	29.8	604.7	48.3	59.7	59.6
(2)	402	398.0	92.8	18.2	287.0	0	59.4	59.0
(3)	45	44.7	30.9	13.3	0.5	0	54.8	53.5
(4)	32	30.1	19.6	10.1	0.4	0	52.6	51.5
(5)	0	3.3	1.2	2.1	0	0	44.0	36.6
(6-A)	0	0.10 ± 0.03	0.04	0.06	0	0	20.3	–
(6-B)	0	0.06 ± 0.03	0.02	0.04	0	0	–	19.5

Table 3: *The numbers of events after each cut for the data and the expected background for the tau channels. The background estimate is normalised to 10.0* pb^{-1}. *The quoted errors are statistical. The last two columns show the selection efficiencies, for cases A and B, for a 65 GeV Higgs boson. The small discrepancy between the data and the total backgrounds in the first line is due to an incomplete modelling of two-photon processes.*

6 The Electron and Muon Channels

The $\ell^+\ell^-q\bar{q}$ (ℓ = e or μ) final states arise mainly from the process $e^+e^-\to Z^0H^0\to\ell^+\ell^-q\bar{q}$, with a branching ratio of approximately 6%, but the $e^+e^-q\bar{q}$ final state includes a small contribution from the fusion process $e^+e^-\to e^+e^-H^0\to e^+e^-q\bar{q}$ (2.4% relative contribution, for m_{H^0}=65 GeV). The analysis adopted concentrates on those final states proceeding through the first process. These yield a clean experimental signature in the form of large visible energy, two energetic, isolated, oppositely charged leptons of the same species reconstructing to the Z^0 boson mass, and two energetic hadronic jets. The dominant backgrounds are $Z^0/\gamma^*\to q\bar{q}$ and four-fermion processes.

The selection proceeds as follows:

(1) The selected events are required to have at least six tracks and are reconstructed as four jets, using the Durham algorithm with a cut of $y_{34} > 0.001$ (single electrons or muons are considered as low-multiplicity "jets"). The events must satisfy the relations $|P^z_{\rm vis}| < 100(E_{\rm vis}/\sqrt{s} - 0.4)$ GeV and $E_{\rm vis} > 0.6\sqrt{s}$.

(2) The selected events must contain at least one pair of electrons or muons of opposite charge. Candidate electron and muon pairs are identified in the following way:

(a) In each event, the two most energetic electromagnetic clusters and the two tracks nearest to them in θ-ϕ space are taken as the candidate electron pair. For each electron candidate, at least 90% of its cluster energy must be contained within fewer than eight lead-glass blocks and the associated track momentum must exceed 5 GeV. The specific ionization loss in the tracking chamber, $\mathrm{d}E/\mathrm{d}x$, must be consistent with that expected for an electron, and the ratio of the cluster energy to the track momentum, E/p, must lie between 0.6 and 4.0. Furthermore, at least one of the electron candidates is required to satisfy $E/p < 1.5$.

(b) Muons are identified using standard algorithms [30]. If there are more than two muons in an event, the pair whose invariant mass is nearest to the Z^0 boson mass is taken as the candidate pair.

(3) Both leptons in the candidate pair must have an energy larger than 25 GeV with at least one of them larger than 35 GeV. The energy of an electron candidate is obtained from the associated electromagnetic cluster, while for a muon candidate it is approximated by the track momentum.

(4) The rest of the event, obtained by excluding the candidate lepton pair, is reconstructed as two jets using the Durham algorithm. An explicit lepton isolation cut is made by requiring that each lepton has a transverse momentum, calculated with respect to the nearest jet axis, larger than 10 GeV. In order to suppress $\mathrm{e^+e^-}\to\mathrm{Z}^0/\gamma^* + \mathrm{Z}^0/\gamma^*$ background events, the opening angle of the jet pair is required to be larger than 50°.

(5) The selected events must have a lepton pair with an invariant mass consistent with the Z^0 boson mass. For electrons the invariant mass of the lepton pair must lie between 75 GeV and 105 GeV, while for muons it must lie between 60 GeV and 120 GeV. The differing mass windows take into account the differing resolutions for electrons and muons.

Distributions of $P^z_{\rm vis}$ versus $E_{\rm vis}/\sqrt{s}$ and E_2 versus E_1, where E_1 (E_2) is the energy of the more (less) energetic lepton in the selected pair, are shown in Figures 3 (c) and (d). The numbers of observed and expected events after each stage of the selection are given in Table 4, together with the detection efficiency for a 65 GeV Higgs boson. After all cuts, no data event survives in either channel while 0.06 ± 0.02 events and 0.04 ± 0.03 events are expected in the electron and muon channels, respectively.

The detection efficiencies as a function of the Higgs boson mass are given in Table 5. These are affected by the following systematic uncertainties: Monte Carlo statistics, 1.2% (electron) and 0.9% (muon); uncertainties in the electron (muon) identification, 2.2% (0.4%); uncertainties in the modelling of fragmentation and hadronization, 0.4%; uncertainties in modelling the cut variables excluding lepton identification, 0.5%. Taking these uncertainties as independent and adding them in quadrature results in a total systematic uncertainty of 3.2% for the electron channel and 1.1% for the muon channel (relative errors).

Cut		Data	Total bkg.	$q\bar{q}(\gamma)$	4-ferm.	Efficiency (%) $m_{H^0} = 65$ GeV
Electron	(1)	337	330.0	299.4	30.7	89.9
	(2)	4	6.8	5.0	1.9	68.0
	(3)	0	0.4	0.2	0.2	66.5
	(4)	0	0.2	0.1	0.1	64.8
	(5)	0	0.06 ± 0.02	0.01	0.05	61.6
Muon	(1)	337	330.0	299.4	30.7	82.6
	(2)	31	30.4	27.3	3.1	79.1
	(3)	0	0.5	0.3	0.2	76.3
	(4)	0	0.07	0.03	0.04	72.5
	(5)	0	0.04 ± 0.03	<0.01	0.04	71.1

Table 4: *The numbers of events after each cut for the data and the expected background in the lepton channels. The background estimate is normalized to 10.0* pb^{-1}*. The quoted errors are statistical. The last column shows the selection efficiencies for the processes* $e^+e^- \to (e^+e^-$ *or* $\mu^+\mu^-)$ H^0*, for a 65 GeV Higgs boson.*

7 Mass Limit for the Standard Model Higgs Boson

The signal detection efficiencies and the numbers of expected signal events, as a function of the Higgs boson mass, are summarized for all search channels in Table 5.

The following uncertainties affecting the numbers of expected signal events are common to all search channels: the uncertainty in the integrated luminosity: 0.6%; the uncertainty in the Higgs boson production cross-section [32], which includes that from the collider energy: 1%; the uncertainty of the Higgs decay branching ratios: 2% [5] [32]. Taking these uncertainties as independent and adding them in quadrature results in a systematic error, common to all search channels, of 3% (relative). In estimating the number of expected events for an assumed Higgs boson mass, these uncertainties are added in quadrature to those affecting the individual search channels.

To derive a lower limit on the Higgs boson mass, this search, with one candidate event in the

four-jet channel (m_{H^0}=46.6 $\pm$ 3.1 GeV) and one candidate event in the missing energy channel (m_{H^0}=39.3 $\pm$ 4.9 GeV), is combined with earlier OPAL searches at $\sqrt{s} \approx m_{\mathrm{Z}^0}$ [4], with two low-mass candidates in the missing energy channel ($m_{\mathrm{H}^0} < 25$ GeV) and one candidate event in the muon channel (m_{H^0}=61.2 $\pm$ 1.0 GeV). The expected numbers of Higgs boson events, combining the present and earlier OPAL searches, are listed in the last column of Table 5. These numbers are affected by total uncertainties of approximately 6%.

Figure 4 shows separately the number of expected events for the present search, for previous OPAL searches, and for their sum, as a function of the Higgs boson mass. Also shown is the 95% confidence level upper limit on the number of observed candidate events. In deriving this upper limit, the probability that a candidate event with a given observed mass actually originates from a Higgs boson of arbitrary mass is calculated following Ref. [33]. The calculation takes into account the mass resolution. No background subtraction is performed and the systematic errors are incorporated into the limit according to the method prescribed in Ref. [34]. A lower limit on the Higgs boson mass, of 65.0 GeV, is extracted at the 95% confidence level. Note that the candidate event with the largest mass lies more than three standard deviations below this limit. For this reason, and because of the steepness of the curve describing the number of expected signal events, the limit does not depend on the detailed knowledge of the mass resolution.

m_{H^0} (GeV)	$\mathrm{q\bar{q}H^0}$ $\mathrm{H^0 \to b\bar{b}}$	$\nu\bar{\nu}\mathrm{H^0}$	$\tau^+\tau^-\mathrm{H^0}$ $\mathrm{H^0 \to q\bar{q}}$	$\mathrm{q\bar{q}H^0}$ $\mathrm{H^0 \to \tau^+\tau^-}$	$\mathrm{e^+e^-H^0}$	$\mu^+\mu^-\mathrm{H^0}$	All 161 GeV	Grand total
35	20.5(3.0)	54.2(2.7)	18.5(0.1)	1.8(0.0)	54.8(0.5)	60.7(0.5)	6.8	163.8
40	21.4(2.8)	56.4(2.5)	27.4(0.2)	5.9(0.1)	56.2(0.4)	62.6(0.5)	6.5	102.5
45	22.3(2.6)	57.8(2.3)	30.5(0.2)	8.7(0.1)	57.5(0.4)	64.5(0.4)	6.1	62.5
50	23.3(2.3)	58.3(2.0)	30.3(0.2)	15.5(0.1)	58.8(0.3)	66.3(0.4)	5.2	30.4
55	24.2(2.0)	57.2(1.6)	27.9(0.1)	20.2(0.1)	60.1(0.3)	68.2(0.3)	4.4	15.1
60	25.1(1.6)	53.6(1.1)	24.2(0.1)	21.1(0.1)	61.3(0.2)	70.0(0.2)	3.3	7.8
62	25.4(1.4)	51.3(1.0)	22.6(0.1)	22.0(0.1)	61.7(0.2)	70.6(0.2)	2.9	5.6
64	24.0(1.1)	48.0(0.7)	21.1(0.1)	20.7(0.1)	61.8(0.2)	71.1(0.2)	2.3	3.6
65	22.8(0.9)	46.0(0.6)	20.3 (0)	19.5(0.1)	61.6(0.1)	71.1(0.2)	2.0	3.0
66	21.5(0.7)	43.9(0.5)	19.6 (0)	19.5(0.1)	61.2(0.1)	70.9(0.1)	1.5	2.3
68	19.1(0.4)	38.6(0.3)	18.3 (0)	17.9 (0)	58.7(0.1)	69.4(0.1)	1.0	1.5
70	16.6(0.2)	31.9(0.1)	17.2 (0)	13.6 (0)	51.1 (0)	63.9 (0)	0.4	0.7

Table 5: *Detection efficiencies (in %) and numbers of expected Higgs boson events (between parentheses) for each search channel separately, as a function of the Higgs boson mass. The last two columns show the total numbers of expected events in the present search at 161 GeV, and the grand total, which also includes the expectations from earlier OPAL searches at centre-of-mass energies close to the* Z^0 *mass.*

8 Summary

A new search is presented for the Standard Model Higgs boson produced in association with a fermion antifermion pair. The search is based on all data collected in 1996 by the OPAL experiment at a centre-of-mass energy of 161 GeV, which correspond to an integrated luminosity of 10.0 pb^{-1}. Combined with earlier OPAL searches at centre-of-mass energies in the vicinity of the Z^0 resonance, this search leads to a lower limit of 65.0 GeV for the mass of the Standard Model Higgs boson, at the 95% confidence level.

Acknowledgements:

We particularly wish to thank the SL Division for the efficient operation of the LEP accelerator at the new energy of $\sqrt{s} = 161$ GeV and for their continuing close cooperation with our experimental group. We thank our colleagues from CEA, DAPNIA/SPP, CE-Saclay for their efforts over the years on the time-of-flight and trigger systems which we continue to use. In addition to the support staff at our own institutions we are pleased to acknowledge the
Department of Energy, USA,
National Science Foundation, USA,
Particle Physics and Astronomy Research Council, UK,
Natural Sciences and Engineering Research Council, Canada,
Israel Science Foundation, administered by the Israel Academy of Science and Humanities,
Minerva Gesellschaft,
Japanese Ministry of Education, Science and Culture (the Monbusho) and a grant under the Monbusho International Science Research Program,
German Israeli Bi-national Science Foundation (GIF),
Bundesministerium für Bildung, Wissenschaft, Forschung und Technologie, Germany,
National Research Council of Canada,
Hungarian Foundation for Scientific Research, OTKA T-016660, and OTKA F-015089.

References

[1] S. L. Glashow, J. Iliopoulos and L. Maiani, Phys. Rev. **D2** (1970) 1285;
S. Weinberg, Phys. Rev. Lett. **19** (1967) 1264;
A. Salam, *Elementary Particle Theory*, ed. N. Svartholm (Almquist and Wiksells, Stockholm, 1968), 367.

[2] P. W. Higgs, Phys. Lett. **12** (1964) 132;
F. Englert and R. Brout, Phys. Rev. Lett. **13** (1964) 321;
G. S. Guralnik, C. R. Hagen, and T. W. B. Kibble, Phys. Rev. Lett. **13** (1964) 585.

[3] ALEPH Collaboration, D. Buskulic *et al.*, CERN-PPE/96-079, submitted to Phys. Lett. **B**;
DELPHI Collaboration, P. Abreu *et al.*, Nucl. Phys. **B421** (1994) 3;
L3 Collaboration, M. Acciarri *et al.*, CERN-PPE/96-095, submitted to Phys. Lett. **B**.

[4] OPAL Collaboration, G. Alexander *et al.*, CERN-PPE/96-118, to be published in Z. Phys. **C**.

[5] A. Djouadi, M. Spira, and P. M. Zerwas, Z. Phys. **C70** (1996) 425.

[6] OPAL Collaboration, K. Ahmet *et al.*, Nucl. Inst. and Meth. **A305** (1991) 275.

[7] P. P. Allport *et al.*, Nucl. Inst. and Meth. **A324** (1993) 34;
P. P. Allport *et al.*, Nucl. Inst. and Meth. **A346** (1994) 476.

[8] B.E. Anderson *et al.*, IEEE Transactions on Nuclear Science **41** (1994) 845.

[9] OPAL Collaboration, K. Ackerstaff *et al.*, CERN-PPE/96-156, to be published in Phys. Lett. **B**.

[10] OPAL Collaboration, R. Akers *et al.*, Phys. Lett. **B327** (1994) 397.

[11] J. Allison *et al.*, Nucl. Inst. and Meth. **A317** (1992) 47.

[12] HZHA generator: P. Janot, in *Physics at LEP2*, edited by G. Altarelli, T. Sjöstrand and F. Zwirner, CERN 96-01, vol. 2 (1996), p. 309.

[13] PYTHIA 5.721 and JETSET 7.408 generators: T. Sjöstrand, Comp. Phys. Comm. **82** (1994) 74; T. Sjöstrand, LU TP 95-20.

[14] EXCALIBUR generator: F.A. Berends, R. Pittau, R. Kleiss, Comp. Phys. Comm. **85** (1995) 437.

[15] BHWIDE generator: S. Jadach, W. Płaczek, B.F.L. Ward, in *Physics at LEP2*, edited by G. Altarelli, T. Sjöstrand and F. Zwirner, CERN 96-01, vol. 2 (1996), p. 286; UTHEP-95-1001.

[16] KORALZ 4.0 generator: S. Jadach, B. F. L. Ward, Z. Wąs, Comp. Phys. Comm. **79** (1994) 503.

[17] PHOJET 1.05 generator: E. Budinov *et al.*, in *Physics at LEP2*, edited by G. Altarelli, T. Sjöstrand and F. Zwirner, CERN 96-01, vol. 2 (1996) p. 216;
R. Engel and J. Ranft, Phys. Rev. **D54** (1996) 4244.

[18] J.A.M. Vermaseren, Nucl. Phys. **B229** (1983) 347.

[19] OPAL Collaboration, G. Alexander *et al.*, Z. Phys. **C52** (1991) 175.

[20] OPAL Collaboration, G. Alexander *et al.*, Phys. Lett. **B376** (1996) 232.

[21] N. Brown and W. J. Stirling, Phys. Lett. **B252** (1990) 657;
S. Bethke, Z. Kunszt, D. Soper and W. J. Stirling, Nucl. Phys. **B370** (1992) 310;
S. Catani *et al.*, Phys. Lett. **B269** (1991) 432;
N. Brown and W. J. Stirling, Z. Phys. **C53** (1992) 629.

[22] G. Parisi, Phys. Lett. **B74** (1978) 65;
J. F. Donoghue, F. E. Low and S. Y. Pi, Phys. Rev. **D20** (1979) 2759.

[23] OPAL Collaboration, R. Akers *et al.*, Z. Phys. **C65** (1995) 17.

[24] OPAL Collaboration, R. Akers *et al.*, Z. Phys. **C66** (1995) 19.

[25] HERWIG generator: G. Marchesini *et al.*, Comp. Phys. Comm. **67** (1992) 465.

[26] ARIADNE generator: L. Lönnblad, Comp. Phys. Comm. **71** (1992) 15.

[27] The grc4f 1.0 generator: J. Fujimoto *et al.*, KEK-CP-046, hep-ph/9603394, to be published in Comp. Phys. Comm.;
J. Fujimoto *et al.*, in *Physics at LEP2*, edited by G. Altarelli, T. Sjöstrand and F. Zwirner, CERN 96-01, vol. 2 (1996) p. 30.

[28] OPAL Collaboration, G. Alexander *et al.*, Z. Phys. **C70** (1996) 357.

[29] OPAL Collaboration, R. Akers *et al.*, Phys. Lett. **B327** (1994) 411.

[30] OPAL Collaboration, G. Alexander *et al.*, Z. Phys. **C52** (1991) 175.

[31] OPAL Collaboration, R. Akers *et al.*, Z. Phys **C63** (1994) 197.

[32] E. Gross, B. A. Kniehl, and G. Wolf, Z. Phys. **C63** (1994) 417;
erratum *ibid.* **C66** (1995) 32.

[33] E. Gross and P. Yepes, Int. Journ. Mod. Phys. **A8 3** (1993) 407.

[34] R. D. Cousins, V. L. Highland, Nucl. Inst. and Meth. **A320** (1992) 331.

OPAL

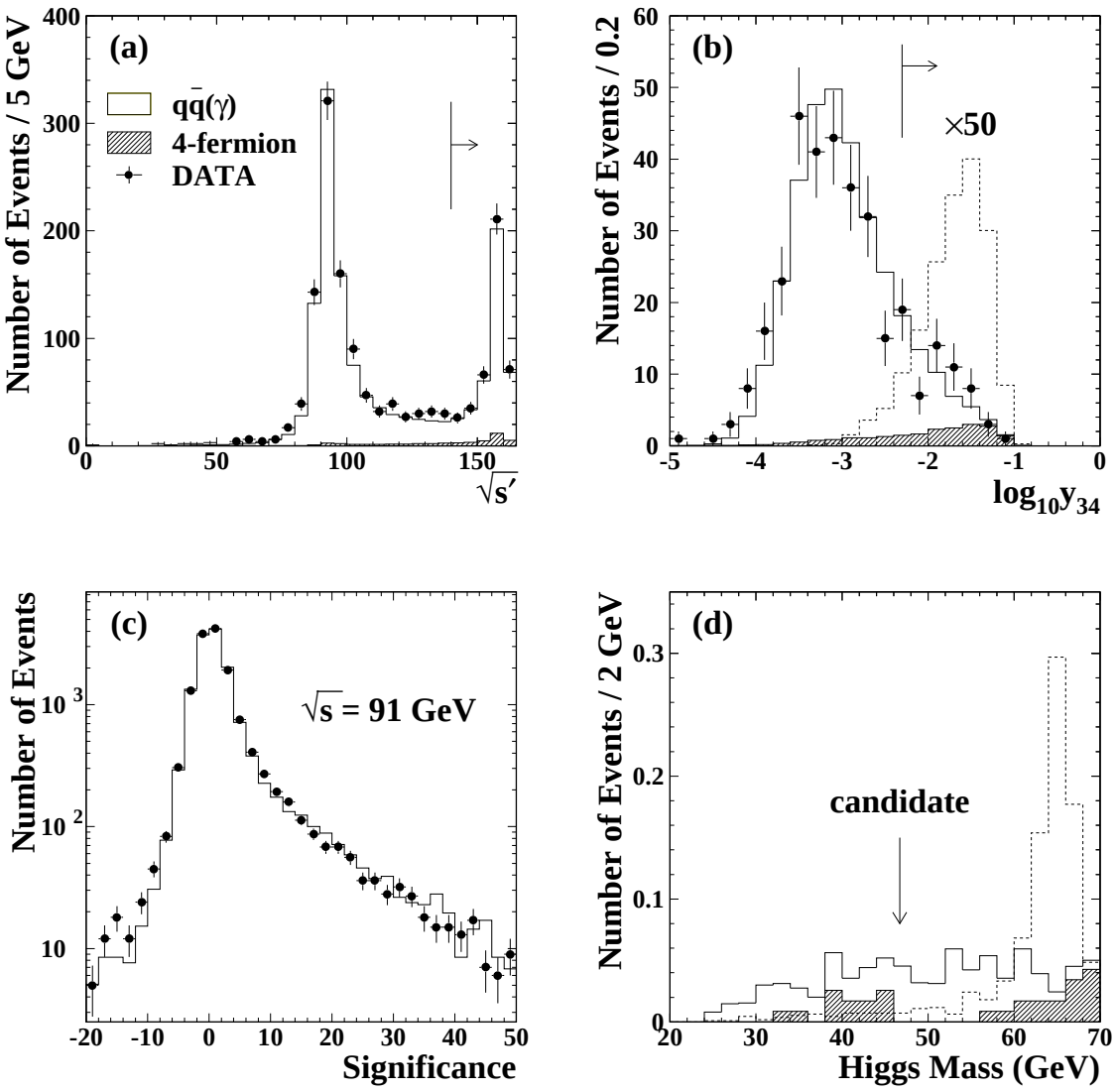

Figure 1: *The four-jet channel; distributions for the data (points with error bars), the background from* $Z^0/\gamma^* \to q\bar{q}$ *(open histograms) and from four-fermion processes (hatched histograms). (a) The* $\sqrt{s'}$ *distribution after cut (1); (b) the* $\log_{10} y_{34}$ *distribution after cut (2); (c) the distribution of the sum of decay-length significances for secondary vertices identified in* Z^0 *decays (the calibration data taken in 1996 at* $\sqrt{s} = 91$ *GeV are shown together with a corresponding* $Z^0 \to q\bar{q}$ *Monte Carlo sample); (d) the invariant mass of the jets assigned to the Higgs boson, after all cuts. In (a) and (b), the arrows indicate domains accepted by the cuts. In (b) and (d), the distributions for a 65 GeV Higgs boson signal are shown by the dotted histograms (in (b) the distribution is scaled by a factor 50 for better visibility). In (d) the arrow indicates the mass of the one candidate event.*

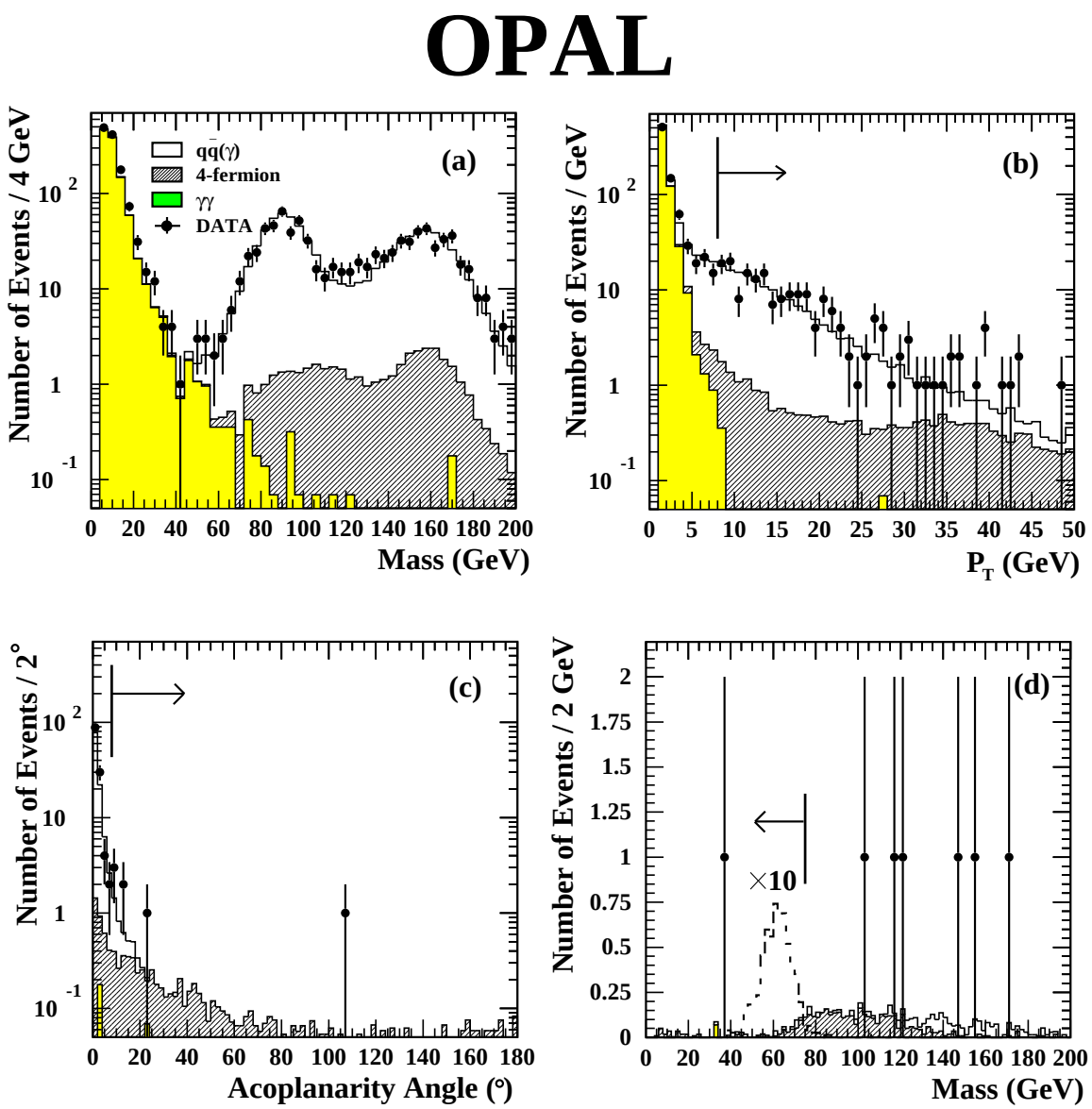

Figure 2: *The missing energy channel; distributions for the data (points with error bars) and for backgrounds expected from two-photon processes (shaded), four-fermion processes (hatched) and* $Z^0/\gamma^* \to q\bar{q}$ *(open histogram). The arrows indicate domains accepted by the cuts. (a) Visible mass distribution after cut (1); (b)* $P^T_{\rm vis}$ *distribution after cut (3); (c) acoplanarity angle distribution after cut (5); (d) distribution of the observed mass after cut (6). In (d), the signal expected from a 65 GeV Higgs boson, scaled by a factor 10 for better visibility, is shown by the dotted line histogram.*

OPAL

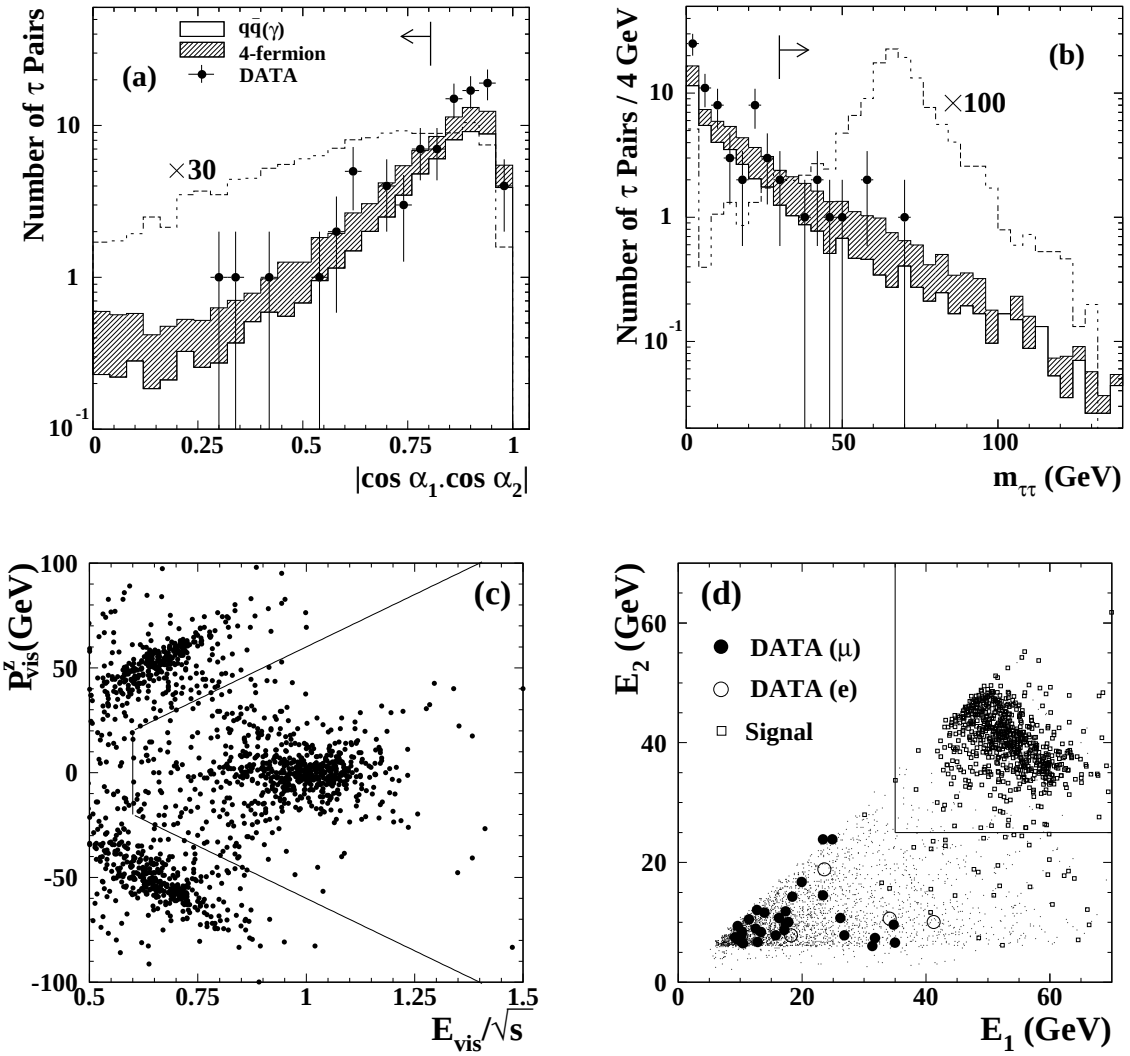

Figure 3: *Parts (a) and (b), tau channels; distributions of the pairwise isolation parameter (see text) after cut (3) and of the $\tau^+\tau^-$ invariant mass after cut (4). Data: dots with error bars; backgrounds: as indicated in (a). The distributions for a 65 GeV Higgs boson from the process $Z^0H^0 \to q\bar{q}\tau^+\tau^-$, scaled up for better visibility, are shown by the dashed histograms. The arrows indicate domains accepted by the cuts. All simulated distributions are normalized to a luminosity of 10.0 pb^{-1}. Parts (c) and (d), electron and muon channels; (c): scatter plot, for the data after selection (2), of $P^z_{\rm vis}$ versus $E_{\rm vis}/\sqrt{s}$. The two clusters at low visible energy and $P^z_{\rm vis} \approx \pm 50$ GeV are from the process $e^+e^- \to Z^0\gamma$ with the photon escaping detection; they are eliminated by the cut indicated by the straight lines (see text: cut (1)). (d): Scatter plot of the energies of the two lepton candidates, after cut (2). The solid lines indicate the positions of cut (3). Large open (filled) dots: electron (muon) candidate events; small dots: predicted background; open squares: distribution for a 65 GeV Higgs boson signal.*

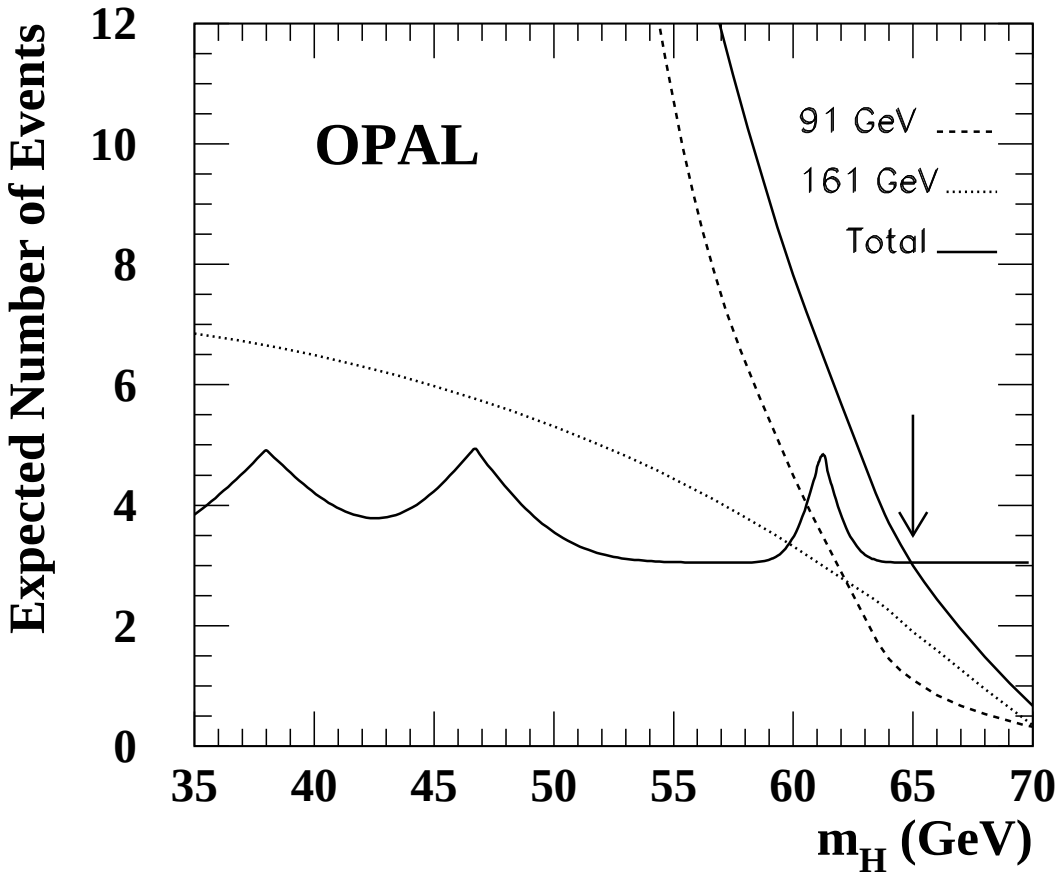

Figure 4: *Expected number of events as a function of the Higgs boson mass. Dotted curve: present search, at 161 GeV centre-of-mass energy; dashed curve: previous OPAL searches, at centre-of-mass energies in the vicinity of the* Z^0 *resonance; steeply falling solid curve: OPAL searches combined. "Horizon-like" solid curve: 95% confidence level upper limit for a possible Higgs boson signal in the presence of three observed high-mass candidate events (see text). The intersection of the two solid curves, indicated by the arrow, determines the 95% confidence level lower limit obtained for the Higgs boson mass.*